Composites Science and Technology 136 (2016) 85–93

Contents lists available at ScienceDirect

Composites Science and Technology

journal homepage: http://www.elsevier.com/locate/compscitech

Oriented bacterial cellulose-soy protein based fully 'green' nanocomposites

Muhammad M. Rahman, Anil N. Netravali*

Department of Fiber Science & Apparel Design, Cornell University, 37 Forest Home Drive, Ithaca, NY 14853, USA

ARTICLE INFO

Article history:
Received 8 June 2016
Received in revised form
14 September 2016
Accepted 4 October 2016
Available online 5 October 2016

Keywords:
Polymers
Nano composites
Mechanical properties
Strength
Bacterial cellulose

ABSTRACT

Bacterial cellulose (BC) nanofibrils are considered as promising biodegradable fiber-reinforcement for polymeric composites because of their excellent tensile properties. However, commonly obtained randomly-oriented web-like form of BC nanofibrils impedes achieving their full potential as reinforcement. In the present study, a facile and scalable method has been developed to orient the nanofibrils through a controlled stretching of BC hydrogel. An optimum hydrogel-stretching at the cross-head speed of 0.05 mm/min and strain ratio of 1.2 showed substantial improvements in the orientation and mechanical properties of BC. Degree of orientation, apparent Young's modulus and fracture stress of the dried BC were increased by 117, 103 and 85%, respectively. Consequently, a BC-reinforced soy protein isolate based fully 'green' composites (BC-SPI composites) were prepared by using vacuum-assisted SPI resin impregnation into BC hydrogel and then stretching the resin impregnated BC hydrogel. The stretched BC-SPI green composites, after drying and curing, showed significant improvement in their tensile properties due to higher BC nanofibrillar orientation. This study opens up new possibilities for direct fabrication of lightweight and mechanically robust 'green' composites that can replace traditional non-degradable composites and reduce carbon footprint significantly.

1. Introduction

Bacterial cellulose (BC) nanofibrils have attracted much attention as composite reinforcement for a variety of applications because of their unique characteristics, such as excellent mechanical properties, low density, low thermal expansion, high optical transparency, and biodegradability [1–3]. BC is an extracellular cellulose produced by Gram-negative aerobic bacterium '*Acetobacter xylinum*' at the air-liquid interface of the culture medium containing carbon and nitrogen sources [4]. Under static cultivation conditions, BC is formed as a multilayer hydrogel scaffold with randomly-oriented ribbon-shaped nanofibrils stacked in a reticulated fashion [5]. One of the advantages of BC over typical cellulose reinforcements from plant sources is that it is extremely pure and does not contain any hemicellulose, lignin, pectin or waxy materials [5]. Furthermore, it has higher crystallinity, degree of polymerization, specific surface area, aspect ratio, and hence, higher tensile properties compared to typical cellulose materials [6,7]. As a result, BC can be successfully exploited in the fabrication of lightweight and strong 'green' composites that can replace petroleum-derived non-degradable composites.

Mechanical properties of BC are known to be affected by several intrinsic and extrinsic factors, such as crystallinity, degree of polymerization, aspect ratio and orientation of the nanofibrils [8]. While some factors can be manipulated by adjusting carbon and nitrogen sources in the culture medium to improve the tensile properties, nanofibrillar orientation cannot be easily obtained as the bacteria move freely in all directions resulting in randomly-oriented nanofibrils in the pellicle. It is commonly known that polymeric composites with uniaxially oriented fibers have better mechanical properties in comparison to those that lack fiber orientation [9,10]. On the same basis, substantial improvement in mechanical performance of BC-reinforced composites should be possible if increased BC nanofibril orientation can be obtained. Although there have been some attempts to produce oriented BC [11–14], no study has been conducted on the implications of oriented BC in composite materials to the best of our knowledge. The reported approaches for orientation could be time consuming and technically complex when the oriented BC are considered for fabricating composite materials on commercial scale [11–13]. It is,

* Corresponding author.
E-mail address: ann2@cornell.edu (A.N. Netravali).

http://dx.doi.org/10.1016/j.compscitech.2016.10.003
0266-3538/

therefore, important to develop a facile, inexpensive, green and scalable process to fabricate oriented BC and oriented BC-reinforced composites.

Plant proteins, by-products after oil extraction from many seeds and grains, have been utilized as bio-based resins for 'green' composites [15–20]. Among them, soy protein is one of the most widely available and comes with several other benefits such as low cost, biodegradability, bio-compatibility, environmental-friendliness and annual renewability [21,22]. Bio-based resins used to fabricate BC-reinforced 'green' composites should meet other critical criteria, such as hydrophilicity, appropriate viscosity, good adhesion to fibers and wettability that soy protein can satisfy [23–26]. The viscosity of hydrophilic soy protein resin can be easily adjusted by altering solution concentration through controlling the amount of water. In addition, it has high affinity to hydroxyl groups on cellulose due to the presence of various polar amino acids [16,23,24].

The present study discusses a simple way to orient BC nanofibrils and fabricate BC-reinforced soy protein isolate (BC-SPI) composites using an inexpensive, green, and scalable process. The first part of this paper discusses BC hydrogel stretching at optimum cross-head speed and strain ratio to obtain the nanofibrillar orientation. Stretched BC was characterized to determine the effect of the stretching process on its morphology, orientation and tensile properties. The second part of the paper discusses similar stretching process used to orient BC-SPI composites prepared via vacuum-assisted resin impregnation and the effects of stretching on the tensile properties of the composites. The morphology, orientation, and tensile properties of the BC and BC-SPI composites were evaluated by wide-angle X-ray diffraction (WAXD), field-emission scanning electron microscopy (FESEM), and uniaxial tensile testing, respectively.

2. Experimental details

2.1. Materials

Acetobacter xylinum strain, ATCC 23769 was obtained from American Type Culture Collection (ATCC, Manassas, VA). D-mannitol, yeast extract and tryptone were purchased from Fisher Scientific (Pittsburgh, PA). SPI was provided by Archer Daniels Midland Co. (Decatur, IL). Analytical grade sodium hydroxide (NaOH) pellets and ammonium nitrates (NH_4NO_3, ≥98% purity) were purchased from Sigma-Aldrich Chemical Co. (Allentown, PA).

2.2. Preparation of BC hydrogel

BC hydrogel in pellicle form (BC-HP) was prepared according to a previously described method with some minor modifications [27]. *Acetobacter xylinum* strain was maintained on agar plates containing 2.5% (w/v) D-mannitol, 0.5% (w/v) yeast extract, 0.5% (w/v) tryptone, and 2.0% (w/v) agar. The strain from the agar plate was transferred into a sterilized culture medium containing the same amount of D-mannitol, yeast extract and tryptone to produce seed culture. This seed culture (~15 mL) was inoculated into a 150 mL culture medium for the production of BC-HP, and the cultivation was carried out at pH of 5.0 ± 0.2 and at 29 °C for 10 days in an incubator. BC-HP produced at the air/culture medium interface was taken out, washed with 1 N NaOH solution at 90 °C for 15 min followed by de-ionized (DI) water at room temperature (RT) to eliminate the cells and chemicals of the culture medium, and stored in DI water at 4 °C for further experiments.

2.3. Stretching of BC hydrogel strips

Rectangular BC hydrogel strips (BC-HS) with dimensions of 15 mm × 60 mm were cut from the BC-HP. Stretching of BC-HS was carried out using Instron universal tensile testing machine (Instron, Model 5566, Canton, MA) in a conditioning room maintained at American Society for Testing and Materials (ASTM) conditions of 65 ± 2% RH and 21 ± 1 °C. BC-HS were stretched with a gauge length of 30 mm at a controlled cross-head speed of 0.05 mm/min until the strain reached 20% or corresponding strain ratio of 1.2. The stretching was stopped at that time, and the stretched BC-HS were kept in between two polyvinylidene fluoride (PVDF) filter papers (Durapore® membrane filters, Filter type: 0.45 μm, Merck Millipore Ltd., Ireland) and cardboards for drying at 50 °C for about 8 h. These dried and stretched BC-HS are referred to as 'Stretched BC' in this study. Un-stretched BC-HS were dried using same process and will be referred to as 'Control BC'.

2.4. Preparation of BC-SPI composites

BC-SPI composites were prepared in water. At first, SPI powder was homogenized in DI water at a ratio of 1:16 (w/v) by a magnetic stirrer for 15 min at RT and further stirred for 20 min at 80 °C by adjusting pH to 10.5 ± 0.2 using a 1 N NaOH solution. Then, BC-HS specimens (Dimensions: 15 mm × 60 mm) cut from the BC-HP were impregnated with SPI resin solution under a vacuum of −0.1 MPa at RT for 30 min in a vacuum oven. SPI-impregnated BC-HS specimens were withdrawn from vacuum oven, and the excess resin from the surface was removed using filter papers. Finally, they were dried at 50 °C for about 8 h and cured by a hydraulic hot-press (Carver Inc., Wabash, IN) at 120 °C for 3 min under a pressure of 8.5 MPa. Dried and cured SPI-impregnated BC-HS specimens will be referred to as 'Control BC-SPI' composites in this study.

2.5. Stretching of SPI-impregnated BC-HS

The stretching process used for BC-HS was performed on the stretching of SPI-impregnated BC-HS. After stretching, the specimens were dried and cured using similar process mentioned in the previous section for the preparation of control BC-SPI composite. These specimens will be referred to as 'Stretched BC-SPI' composites.

2.6. Characterization

WAXD patterns of control and stretched BC specimens were recorded using Bruker AXS Hi-star general area detector diffractometer (Madison, WI) equipped with Cu$K\alpha_1$ radiation ($\lambda = 0.154$ nm) operated at 40 kV and 20 mA. Azimuthal intensity distribution pattern for (200) equatorial reflection was used to calculate degree of orientation (DO) according to the equation: $DO = \frac{180^\circ - FWHM}{180^\circ}$; where, FWHM represents full width at half-maximum of the azimuthal profiles from the equatorial reflection [10].

Tensile properties of all specimens were determined using the same Instron, equipped with a 100 N load cell. All specimens had dimensions of 5 mm × 50 mm (Width × Length). The thicknesses of the specimens was measured by a digimatic micrometer (Model: MDC-1 PJ, Mitutoyo, Japan) and were found to be in the range of 0.3–0.4 mm. Sheets having 10 mm × 10 mm dimensions were weighed to calculate the density. Each specimen was glued between two rectangular paper tabs keeping the gauge length of 20 mm and subsequently tested using a cross-head speed of 0.4 mm/min. The apparent Young's modulus values were calculated in the range of 0.1–1.0% strain from the stress-strain plots. All specimens were conditioned at a temperature of 21 ± 1 °C and a

relative humidity (RH) of 65 ± 1% for 24 h using a saturated NH_4NO_3 solution before the tensile test. A minimum of six specimens were tested to obtain average values and standard deviations. Statistical analyses were performed using JMP statistical software (SAS Institute, Cary, NC).

The weight fraction of BC in control and stretched BC-SPI composites was calculated by SPI resin dissolution. The specimens (20 mm × 20 mm) were weighed and submerged into a bath of alkaline solution (pH~10.5) for about 24 h maintained at 80 °C. After 24 h when the SPI resin was disintegrated completely, BC was taken out and washed several times using DI water. The BC was then dried at 50 °C for 6 h and weighed to calculate the weight fraction in the composite.

Fracture surfaces after tensile test and through-plane surfaces of all specimens were analyzed using a Tescan Mira3 FESEM (Tescan USA, Inc., Warrendale, PA) at an accelerating voltage of 3 kV. The surfaces were coated with a thin layer of gold to prevent charging using a Denton Desk V sputter coater (Denton Vacuum, Moorestown, NJ) before observation.

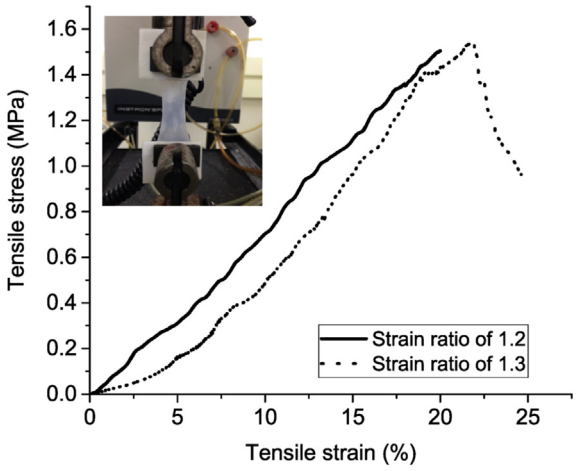

Fig. 1. Typical stretching behavior of BC-HS at a cross-head speed of 0.05 mm/min. Inset photograph shows the BC-HS specimen being stretched on Instron.

3. Results and discussion

BC-HP is a highly porous membrane composed of three-dimensional cellulosic fibrous network with a substantial amount of interstitial water [28]. BC-HP, in this study, contained around 98% water and 2% BC nanofibrils that were oriented randomly without any restriction in their native state. In this state, while the maximum inelastic deformation upon tensile stretching can be expected due to the inherent lubrication effect of the interstitial water, nanofibril entanglements restrict the deformation. Water has been considered as one of the most efficient lubricants for wet-spinning of various hydrophilic polymers [10]. With abundance of water as lubricant in BC-HP, it can be expected that the nanofibrils could move easily and orient themselves in the direction of the stress during the stretching process. In this process, initially, the inter-nanofibril distance reduces as the pore volume decreases upon stretching while the reduction in inter-nanofibril distance increases the inter-nanofibrillar hydrogen bonding. Further stretching can generate twisting and firmer interlocking among the already entangled nanofibrils restricting the nanofibrillar rearrangement in the BC network. However, loosely entangled nanofibrils try to get straightened in the stress direction until fully constrained, with increased stretch. Stretching beyond this point initiates nanofibril fracture degrading the tensile properties of the BC network. In all phases of stretching, as nanofibrils come closer the interstitial water from the BC network gets squeezed out, resulting in an irreversible formation of hydrogen bonds between BC nanofibrils [13]. Therefore, lateral shrinkage of the specimen with maximum orientation in the stretching direction can be expected.

It is critical to determine the maximum stretching possible while avoiding any damage to the fibrous network so as to be able to utilize the full potential of the oriented nanofibrils. To achieve that, two limiting factors, namely, cross-head speed and strain ratio need to be optimized to achieve highest possible orientation of nanofibrils. Hence the word 'optimized' in this study only refers to the best combination of strain rate and strain ratio. Higher cross-head speed and/or strain ratio can inevitably lead to premature nanofibril fracture. Therefore, some preliminary experiments were performed to determine optimum strain ratio and cross-head speed that allowed largest inelastic deformation of BC-HS and obtain best possible orientation of the BC nanofibrils. Fig. 1 shows the typical stress-strain plot of BC-HS being stretched at a cross-head speed of 0.05 mm/min and the inset photograph shows a BC-HS specimen being stretched on an Instron. As shown in Fig. 1, the optimum stretching of BC-HS was observed at a strain ratio of 1.2. Optimum stretching in this case is defined as the maximum stretch (strain) that can be reached without the initiation of fracture in the BC nanofibrillar network. Stretching to higher strain ratios (strain ratio >1.2), however, showed fracture of the hydrogel nearly in all cases, as shown in Fig. 1, for strain ratio of 1.3. The achievable strain ratio in BC-HS was found to be limited due to the high density of entanglements between nanofibrils which impede each other to be perfectly aligned upon stretching. However, lower cross-head speed was found to be better for controlled stretching up to the maximum possible strain ratio. The cross-head speed was set to 0.05 mm/min based on the preliminary experiments. Lower cross-head speed provides sufficient time for maximum rearrangement and reduces the stress on nanofibrils [10]. However, extremely low cross-head speed of less than 0.05 mm/min had a drying effect due to the large timescale needed for stretching. Hence, the strain ratio of 1.2 and cross-head speed of 0.05 mm/min were considered as providing maximum possible nanofibrillar alignment for BC-HS in this study.

The effect of stretching on the orientation of BC nanofibrils was evaluated using WAXD analysis. WAXD images were collected in both perpendicular and parallel directions to the control and stretched BC plane to analyze any change in the nanofibrillar orientation resulting from stretching. The BC plane perpendicular to the X-ray beam is referred to as through-plane (TP) direction while BC plane was aligned parallel to the X-ray beam in the cross-section (CS) direction. Fig. 2 shows WAXD images of the crystallographic lattice planes in the TP and CS directions of control and stretched BC. As can be seen in Fig. 2, a significant change in the ring pattern was observed at the (200) equatorial reflection of BC due to nanofibrillar rearrangement after stretching. Control BC shows a ring pattern along the TP direction indicating random orientation of the BC nanofibrils (Fig. 2a). In comparison, equatorial arc pattern formed along the TP direction of stretched BC is confined to sharp spots as seen in Fig. 2b, suggesting a preferred orientation along the stretching direction. In the CS direction, the formation of diffraction spots is more prominent compared to TP direction (Fig. 2c-d) and hence, the effect of stretching on the orientation of the nanofibrils is more pronounced.

DO was quantified from the azimuthal intensity profiles from WAXD of control and stretched BC. Fig. 3 shows the azimuthal intensity profiles at the (200) equatorial reflection for TP and CS directions of the control and stretched BC and Fig. 4 shows the degree of orientation for TP and CS views, respectively. DO ranges between

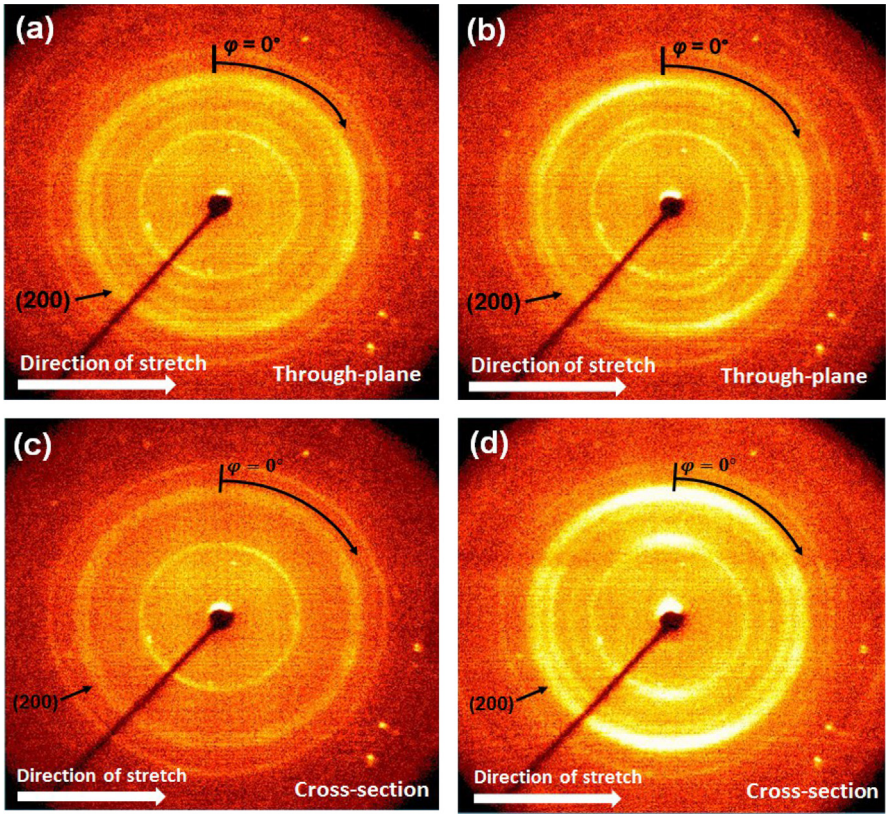

Fig. 2. WAXD images: through-plane view of (a) control, (b) stretched BC and cross-section view of (c) control, (d) stretched BC.

0 and 1 where DO of 1 corresponds to perfect orientation parallel to stretching direction and DO of 0 refers to perfectly random orientation. As can be seen in Fig. 4, the degree of orientation of stretched BC is significantly higher compared to control BC in both TP and CS directions. For control BC the degree of orientation was 0.29 and 0.38 in TP and CS directions, respectively, whereas the values of stretched BC in the two directions were 0.63 and 0.71, respectively. The narrower and more defined intensity maxima in comparison to the control BC (Fig. 3) indicated the preferred orientation of nanofibrils along the stretching direction.

The surfaces of control and stretched BC specimens were observed by FESEM to characterize the effect of stretching on surface morphology and orientation. Fig. 5 shows the FESEM images of the surfaces of control and stretched BC. As can be seen in Fig. 5a, the surface of control BC showed a comparatively high degree of roughness while stretched BC had a smoother surface (Fig. 5b). The quantitative values of the surface roughness were measured using an optical interferometer (ADE Phase Shift MicroXAM Optical interferometric profiler). The roughness values were found to be 3.8 ± 0.4 μm and 1.9 ± 0.3 μm for control BC and stretched BC, respectively. The formation of smoother surface is attributed to the evening out due to stretching. The higher magnification image of control BC (Fig. 5c) clearly showed the random orientation of the nanofibrils whereas after stretching, a significant number of nanofibrils were observed to be better oriented in the direction of stretching (Fig. 5d) supporting the WAXD observations. Many of the nanofibrils were partially orientated and were inclined at some angles with the stretching direction and only a small fraction of the nanofibrils were almost perpendicular to the stretching direction. This is clearly due to large number of entanglements among the nanofibrils which limit the strain ratio as discussed earlier. Qualitative observation of FESEM images showed a significant difference in porosity due to stretching of BC network. Pore diameters ranged from several dozen to several hundred nanometers and very irregular shape in a high-density network for control BC (Fig. 5c) while the pore diameter and shape irregularity reduced substantially due to the decrease in inter-fibrillar angles and fiber-fiber gap along the stretching axis for stretched BC (Fig. 5d).

Fig. 6 shows typical tensile stress-strain plots of control and stretched BC while Table 1 presents the average values for apparent Young's modulus, fracture stress, and fracture strain obtained from the plots. As seen in data presented in Table 1, apparent Young's modulus and fracture stress of stretched BC increased substantially. These were accompanied by a significant decrease in fracture strain as can be expected. Compared to control BC, apparent Young's modulus was increased by approximately 103% (from 3.2 GPa to 6.5 GPa) and fracture stress was increased by about 85% (from 71.3 MPa to 132 MPa) after stretching as a result of enhanced nanofibrillar orientation. The same factor reduced the fracture strain by about 45% (from 4.5% to 2.5%) in stretched BC as expected. Analysis of variance (ANOVA) revealed the difference in the tensile properties between control and stretched BC to be significant (p-value < 0.05). The major reason for the enhancement of apparent Young's modulus and fracture stress in the stretched BC is the nanofibrillar alignment in the direction of loading [29]. The other practical reason for the increase in apparent Young's modulus and fracture stress might be attributed to the reduction in porosity. It is well-known that porosity is one of the most important structural characteristic of BC [30]. The adverse effect of porosity on the mechanical properties in materials has been discussed by Retegi et al. [30]. Theoretically, the porosity (P) of BC can be calculated from the absolute density of cellulose crystallite ($\rho_t \sim 1.59 g/cm^3$)

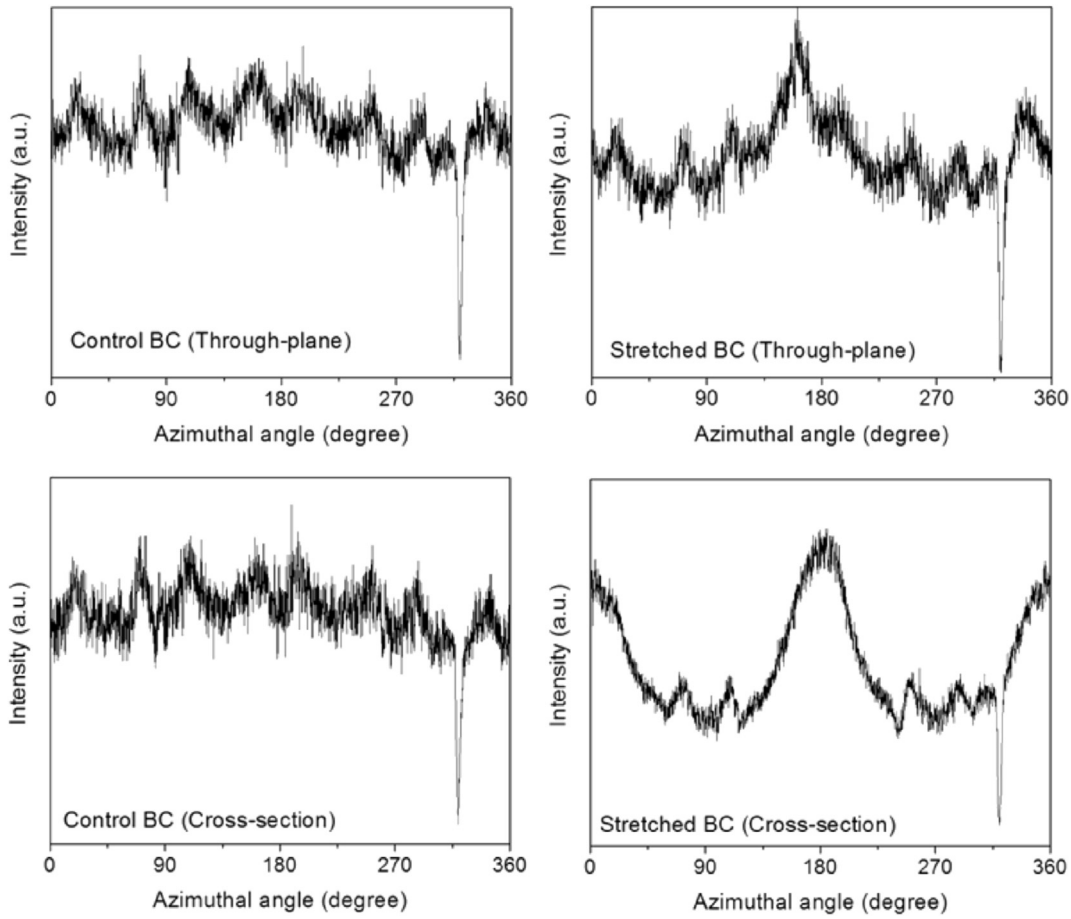

Fig. 3. Azimuthal intensity profiles at the equatorial reflection (200) for through-plane and cross-section directions of control and stretched BC.

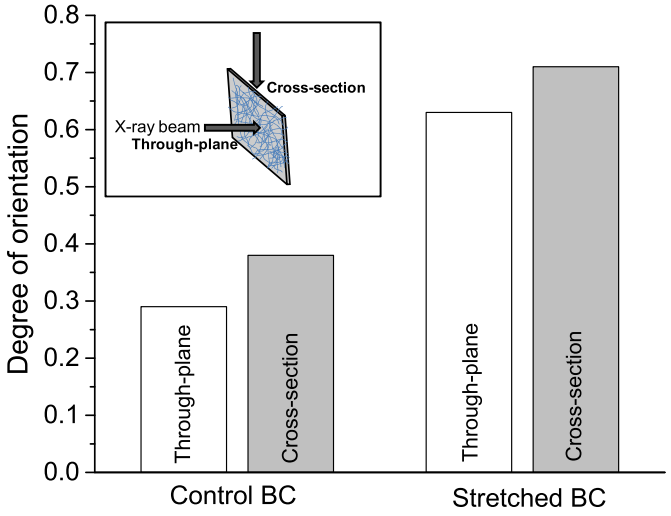

Fig. 4. Degree of orientation for through-plane and cross-section views of control and stretched BC. Inset schematic shows the direction of X-ray beam.

and bulk density (ρ_s) of BC using the equation [30]: $P = \left(\frac{\rho_t - \rho_s}{\rho_t}\right) \times 100\%$. The bulk densities of the control and stretched BC as determined by measuring their volumes and weights were found to be 1.02 g/cm^3 and 1.18 g/cm^3, respectively. The calculated pore volume of the control BC was found to be 36% which accounted for more than one-third of the total volume while the pore volume of stretched BC was reduced to around 26% or one-fourth of the total volume. This result agrees well with the FESEM observations discussed earlier and shown in Fig. 5 (c) and (d). The experimental fracture stress and Young's modulus values were calculated based on the geometrical area of the load resisting or the lowest cross-section within the gauge length. However, the values of such tensile properties can also be determined based on the real area of the load resisting cross-section by considering the pore volume. Taking into consideration the pore volume, fracture stress and Young's modulus can be calculated using the equation [31]: $M = M_a/(1-P)$, where M_a is the experimental property values (fracture stress or Young's modulus) considering the porosity while M is one of the properties (fracture stress/Young's modulus) of the solid material considering there is no porosity and P is the pore volume fraction.

As the next step, fully 'green' composites were developed by filling the pores in the BC with biodegradable SPI resin using vacuum-assisted impregnation process. In a composite material, porosity should be reduced as much as possible since the pores have a negative influence on the stress transfer between fiber and resin [32]. Fig. 7 shows the FESEM images of surfaces of control and stretched BC-SPI composites at different magnifications. As can be seen in Fig. 7, SPI resin fills the pores effectively in both composites. Despite these observations of the micrographs, these composites may still have some porosity which have been calculated according to the equation [33]: Porosity $= \left(1 - \frac{\rho_c}{w_f \rho_f + w_r \rho_r}\right) \times 100\%$, where ρ_c,

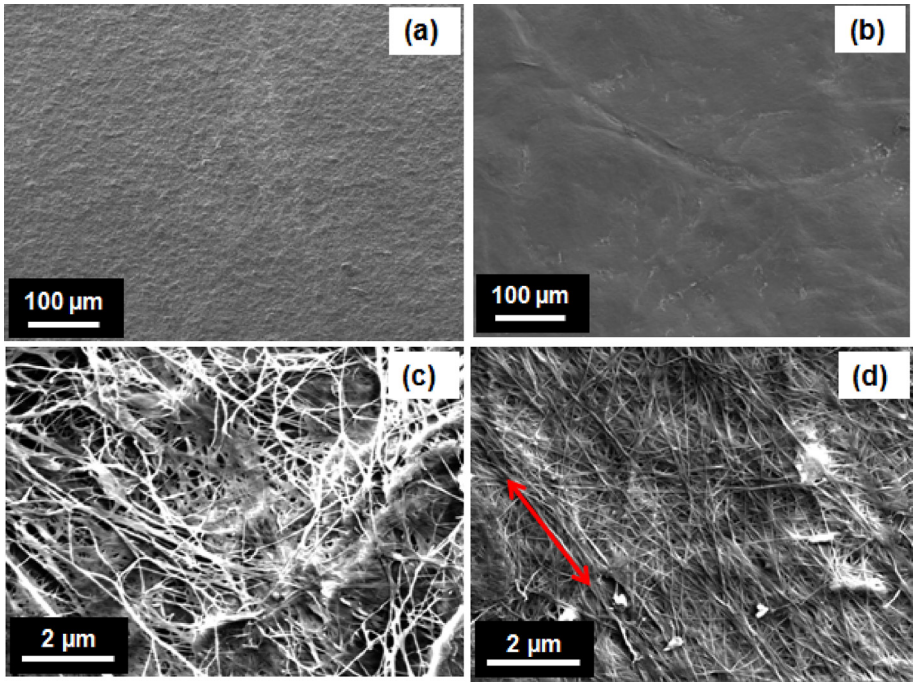

Fig. 5. FESEM images of surfaces of control (a, c) and stretched BC (b, d) at different magnifications.

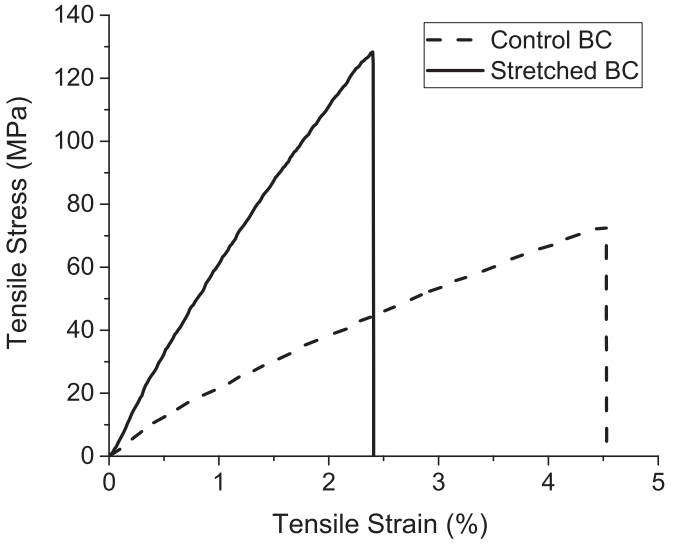

Fig. 6. Typical tensile stress-strain plots of the control and stretched BC.

fiber weight fractions could easily be controlled by simply adjusting the concentration of the SPI solution. Previously, Nakagaito and Yano observed a bi-linear relationship between Young's modulus and fiber content in phenol-formaldehyde/micro-fibrillated cellulose (MFC) composites [34]. They found that increasing MFC content up to 40 wt% resulted in a linear relationship with Young's modulus while above 40 wt% fiber content created a negative deviation from this linear relationship. They described this as the reinforcing saturation effect. Retegi et al. observed difficulties to fill the pores with epoxidized soybean oil resin in acetylated BC at high content in spite of the low viscosity of the resin [35]. This caused inhomogeneity problems in acetylated BC-epoxidized soybean oil composites [35]. Since the effect of fiber content was not the prime concern in this study, the BC content in the composites was maintained at about 40 ± 2% by weight based on the previous studies [34,35]. Here, the effect of stretching on the tensile properties of the BC-SPI composite was investigated and is discussed later.

Typical tensile stress-strain plots of SPI resin, control, and stretched BC-SPI composites are shown in Fig. 8 and Table 2 summarizes Young's modulus, fracture stress, and fracture strain values

Table 1
Tensile properties of control and stretched BC.

Specimen	Apparent Young's modulus (GPa)[a]	Young's modulus (GPa)[b]	Experimental fracture stress (MPa)[a]	Fracture stress (MPa)[b]	Fracture strain (%)
Control BC	3.2 ± 0.4	5.0 ± 0.6	71.3 ± 13.9	111.4 ± 21.8	4.5 ± 0.7
Stretched BC	6.5 ± 0.7	8.8 ± 1.0	132.0 ± 19.5	178.3 ± 25.9	2.6 ± 0.3

[a] Experimental values for porous BC (based on geometrical area).
[b] Recalculated values taking consideration of porosity (based on real area).

ρ_f and ρ_r, are the bulk densities of the composite, BC and SPI, respectively, and w_f, and w_r are weight fractions of BC, and SPI, respectively. The porosities in both composites were calculated to be in the range of 2–3% which may be quite typical.

Since the processing of resin was water-based, the resin and obtained from the plots. The tensile properties of SPI resin included in Table 2 were used to calculate the theoretical values of the composites using rule of mixtures (ROM). As expected, similar effects of stretching on the tensile properties were observed in the case of composites. The stretched BC-SPI composites showed

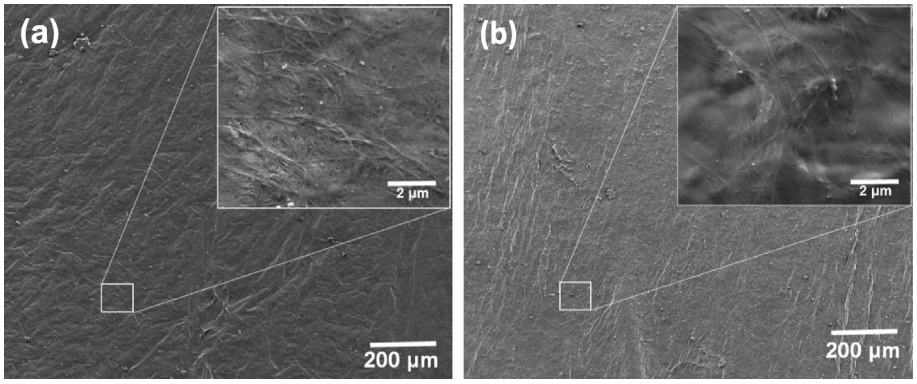

Fig. 7. FESEM images of surfaces of control BC composite (a) and stretched BC composite (b) shown at different magnifications.

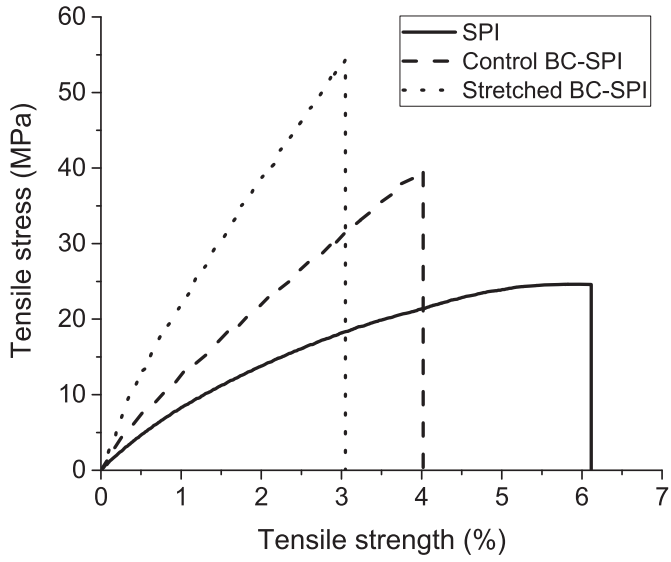

Fig. 8. Typical tensile stress-strain plots of SPI resin, control BC-SPI, and stretched BC-SPI composite.

to be slightly lower as compared to the improvements observed in the BC alone. SPI resin impregnated BC-HS was more difficult to be aligned through stretching compared to BC-HS alone. The main reason for this is the higher viscosity of the impregnated SPI resin impedes the natural movement of the BC nanofibrils, compared to water, and limits their disentanglement and, hence, their orientation.

The theoretical values for Young's modulus and fracture stress of control and stretched BC-SPI composites were calculated using ROM to compare with the experimental values (Table 2) [27]. The ROM model for randomly-oriented fiber composites modified by Cox and Krenchel was used to predict the Young's modulus of the composites since this model has been modified by taking into consideration the effect of fiber length and orientations [36]: $E_c = \eta_l \eta_0 E_f v_f + E_m(1-v_f)$, where E_c, E_f, *and* E_m are Young's modulus values of composite, BC nanofibrils and soy protein resin, respectively, and v_f is the volume fraction of BC nanofibrils in the composites. η_l is a length correction factor for 'short' reinforcing fibers [36]. For continuous fibers, η_l is considered as 1. η_0 is the Krenchel orientation efficiency factor which can be expressed as: $\eta_0 = \sum_1^n a_n cos^4\theta_n$, where, a_n is the ratio between the cross-sectional area presented by a group of fibers orientated at an angle θ_n to the applied load direction and the total area of all the fibers at a given cross-section of the composites. In this study η_0 was taken 0.2 for

Table 2
Tensile properties of SPI resin, control and stretched BC-SPI composite.

Specimen	Young's modulus (GPa)	Fracture stress (MPa)	Fracture strain (%)
SPI resin	0.9 ± 0.2	25.3 ± 4.2	6.5 ± 2.8
Control BC-SPI (Experimental)	1.9 ± 0.3	40.0 ± 7.6	4.2 ± 0.4
Control BC-SPI (Theoretical)[a]	2.5	–	–
Control BC-SPI (Theoretical)[b]	6.9	–	–
Stretched BC-SPI (Experimental)	3.6 ± 0.4	66.3 ± 10.1	2.7 ± 0.3
Stretched BC-SPI (Theoretical)[a]	4.1	–	–
Stretched BC-SPI (Theoretical)[b]	12.5	–	–

[a] Considering the theoretical properties of BC mat and conventional ROM model.
[b] Considering the theoretical properties of single BC fiber and modified ROM (Cox-Krenchel) model.

significantly higher modulus and strength with lower fracture strain compared to control BC-SPI composites. Control BC-SPI composites showed an average Young's modulus of 1.9 GPa, fracture stress of 40 MPa and fracture strain of 4.2%. After stretching, the Young's modulus increased by about 90% to 3.6 GPA and the fracture stress increased by 66% to 66.3% MPa while the fracture strain decreased by about 36% to 2.7%. The improvements in the tensile properties of the composites due to stretching were found

3D randomly-oriented fibers [37]. However, it is very difficult to assume the value of η_0 for the stretched and oriented BC in the present case. For the calculation, the value of 0.375 was used by taking into consideration the orientation distribution at different angles as shown in Fig. 5d and the DO as observed in Fig. 4. The densities of SPI resin and BC nanofibrils used to calculate the theoretical values were 1.27 and 1.59 g/cm^3, respectively [30]. The theoretical predictions and experimental results for Young's

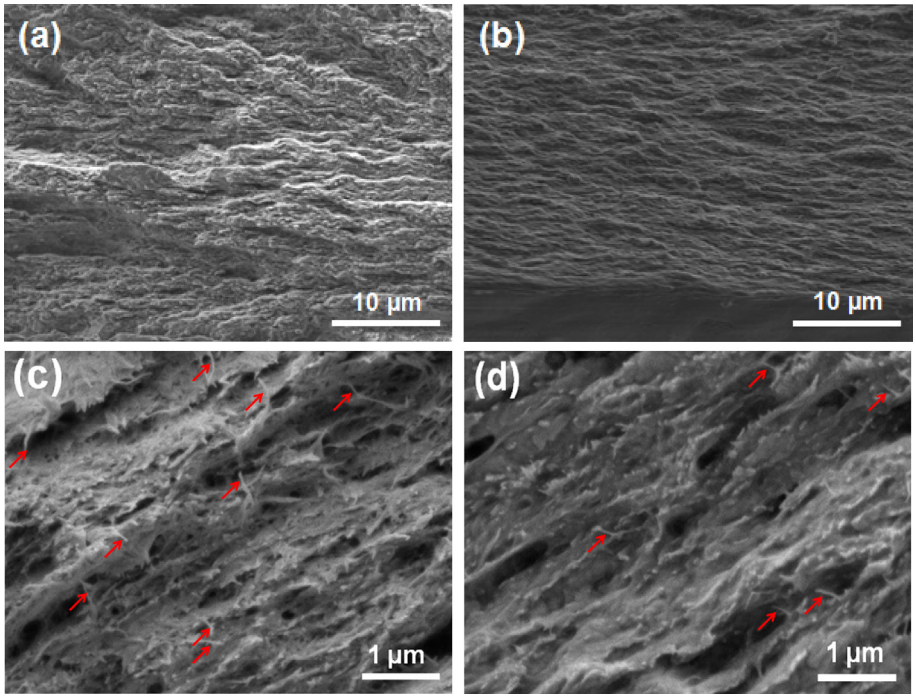

Fig. 9. FESEM images of fracture surfaces of control (a, c), and stretched (b, d) BC-SPI composites at different magnifications after uniaxial tensile test.

modulus values for control and stretched BC are very different from each other while the properties of single BC fiber are considered (Table 2). However, based on the properties of BC mat the theoretical and experimental values for Young's modulus of the composites are very close. The theoretical value of Young's modulus for BC mat, even if BC nanofibrils were aligned, would be much lower compared to a single BC nanofibril as per the bundle theory of fibers [38]. In addition, fiber orientation, another significant factor, should also be considered for calculating the theoretical properties of the composites. The agreement between the theoretical and experimental values for Young's modulus of the BC mat can be attributed to the BC and SPI compatibility in the composites [25,26]. In addition, vacuum-assisted SPI infiltration helps to obtain BC-SPI homogeneity. Overall, the significant enhancements in tensile properties of composites are the result of the increased orientation of the BC nanofibrils.

Fig. 9 shows FESEM images of fracture surfaces of control and stretched BC-SPI composites after the tensile test. More random and undulated layers were observed in the control BC-SPI composites (Fig. 9a) whereas more compact and smooth appearance of layers were observed in stretched BC-SPI composites (Fig. 9b). The more compact layer suggests reduction in the porosity and increase in the orientation due to stretching. Besides, comparatively less featured fracture surface with less interruption of failure propagation was observed in the stretched BC-SPI composite indicating more brittleness. On the contrary, a greater degree of roughness in the control composites indicates greater interruption of failure propagation implying a ductile system. The mechanical properties, e.g., fracture strain, observed during tensile tests agree with the FESEM analysis. As seen in Fig. 9c, some of the BC nanofibrils are protruding out from SPI resin in control BC-SPI composite specimen as indicated by the red arrows. However, less nanofibrillar protrusion from the resin was observed (Fig. 9d) in the stretched BC-SPI composite. The protruding lengths in this case are shorter compared to the control BC-SPI composites. This phenomenon can be explained by the brittle fracture or low fracture strain behavior of the stretched composite. Nanofibrils more aligned with the plane of the fracture surface are easier to be pulled out than those perpendicular to it.

4. Conclusions

In this study, a straightforward process for the fabrication of oriented BC and BC-reinforced 'green' composites by simple hydrogel-stretching, drying and curing has been developed. Although the mechanical (tensile) properties of BC depend on several intrinsic, extrinsic and processing parameters, the effect of orientation has been considered in this study, keeping the other factors constant. An optimum and controlled stretching of BC hydrogel at a cross-head speed of 0.05 mm/min and a strain ratio of 1.2 demonstrated significant improvements in the orientation of randomly-oriented nanofibrils and resulted in significantly higher tensile properties. Similarly, significant improvement in the tensile properties of BC-SPI composite was obtained after similar stretching of SPI-impregnated BC hydrogel, due to nanofibrillar orientation. High density of entanglements in BC networks was seen to impede obtaining perfect alignment through stretching. The entanglements, in the future, may be reduced through the control of microbial movement during the fermentation process. Hence, considering the simplicity of the route and sustainable characteristics of the materials, the process could open up opportunities for the development of mechanically robust and lightweight advanced 'green' composites that can replace traditional non-degradable plastics and composites.

Acknowledgements

The authors would like to acknowledge NSF-CREST grant (1137681) for funding this research. The authors also would like to acknowledge the use of Cornell Center for Materials Research (CCMR) facilities supported by NSF (award no. DMR-1120296).

References

[1] K. Qiu, A.N. Netravali, A review of fabrication and applications of bacterial cellulose based nanocomposites, Polym. Rev. 54 (2014) 598–626, http://dx.doi.org/10.1080/15583724.2014.896018.

[2] H. Yano, J. Sugiyama, A.N. Nakagaito, M. Nogi, T. Matsuura, M. Hikita, K. Handa, Optically transparent composites reinforced with networks of bacterial nanofibers, Adv. Mater 17 (2005) 153–155, http://dx.doi.org/10.1002/adma.200400597.

[3] D. Klemm, B. Heublein, H.-P. Fink, A. Bohn, Cellulose: fascinating biopolymer and sustainable raw material, Angew. Chem. Int. Ed. 44 (2005) 3358–3393, http://dx.doi.org/10.1002/anie.200460587.

[4] X. Shen, J.L. Shamshina, P. Berton, G. Gurau, R.D. Rogers, Hydrogels based on cellulose and chitin: fabrication, properties, and applications, Green Chem. 18 (2015) 53–75, http://dx.doi.org/10.1039/C5GC02396C.

[5] D. Klemm, D. Schumann, U. Udhardt, S. Marsch, Bacterial synthesized cellulose — artificial blood vessels for microsurgery, Prog. Polym. Sci. 26 (2001) 1561–1603, http://dx.doi.org/10.1016/S0079-6700(01)00021-1.

[6] T. Zhang, W. Wang, D. Zhang, X. Zhang, Y. Ma, Y. Zhou, L. Qi, Biotemplated synthesis of gold nanoparticle–bacteria cellulose nanofiber nanocomposites and their application in biosensing, Adv. Funct. Mater. 20 (2010) 1152–1160, http://dx.doi.org/10.1002/adfm.200902104.

[7] R. Mohammadinejad, S. Karimi, S. Iravani, R.S. Varma, Plant-derived nanostructures: types and applications, Green Chem. 18 (2015) 20–52, http://dx.doi.org/10.1039/C5GC01403D.

[8] V. Thiruvengadam, S. Vitta, Bacterial cellulose and its multifunctional composites: synthesis and properties, in: V.K. Thakur (Ed.), Nanocellulose Polym. Nanocomposites, John Wiley & Sons, Inc., 2014, pp. 479–506. http://onlinelibrary.wiley.com/doi/10.1002/9781118872246.ch17/summary (accessed 10.01.2016).

[9] H. Sehaqui, N. Ezekiel Mushi, S. Morimune, M. Salajkova, T. Nishino, L.A. Berglund, Cellulose nanofiber orientation in nanopaper and nanocomposites by cold drawing, ACS Appl. Mater. Interfaces 4 (2012) 1043–1049, http://dx.doi.org/10.1021/am2016766.

[10] J.G. Torres-Rendon, F.H. Schacher, S. Ifuku, A. Walther, Mechanical performance of macrofibers of cellulose and chitin nanofibrils aligned by wet-stretching: a critical comparison, Biomacromolecules 15 (2014) 2709–2717, http://dx.doi.org/10.1021/bm500566m.

[11] T. Kondo, M. Nojiri, Y. Hishikawa, E. Togawa, D. Romanovicz, R.M. Brown, Biodirected epitaxial nanodeposition of polymers on oriented macromolecular templates, Proc. Natl. Acad. Sci. 99 (2002) 14008–14013, http://dx.doi.org/10.1073/pnas.212238399.

[12] A. Putra, A. Kakugo, H. Furukawa, J.P. Gong, Y. Osada, Tubular bacterial cellulose gel with oriented fibrils on the curved surface, Polymer 49 (2008) 1885–1891, http://dx.doi.org/10.1016/j.polymer.2008.02.022.

[13] A. Putra, A. Kakugo, H. Furukawa, J.P. Gong, Y. Osada, T. Uemura, M. Yamamoto, Production of bacterial cellulose with well oriented fibril on PDMS substrate, Polym. J. 40 (2008) 137–142.

[14] A. Putra, A. Kakugo, H. Furukawa, J.P. Gong, Orientated bacterial cellulose culture controlled by liquid substrate of silicone oil with different viscosity and thickness, Polym. J. 41 (2009) 764–770, http://dx.doi.org/10.1295/polymj.PJ2009023.

[15] S. Chabba, G.F. Matthews, A.N. Netravali, “Green” composites using cross-linked soy flour and flax yarns, Green Chem. 7 (2005) 576, http://dx.doi.org/10.1039/b410817e.

[16] X. Huang, A. Netravali, Biodegradable green composites made using bamboo micro/nano-fibrils and chemically modified soy protein resin, Compos. Sci. Technol. 69 (2009) 1009–1015, http://dx.doi.org/10.1016/j.compscitech.2009.01.014.

[17] T.G. Dastidar, A.N. Netravali, A soy flour based thermoset resin without the use of any external crosslinker, Green Chem. 15 (2013) 3243–3251, http://dx.doi.org/10.1039/C3GC40887F.

[18] M.M. Rahman, A.N. Netravali, B.J. Tiimob, V.K. Rangari, Bioderived “green” composite from soy protein and eggshell nanopowder, ACS Sustain. Chem. Eng. 2 (2014) 2329–2337, http://dx.doi.org/10.1021/sc5003193.

[19] M.M. Rahman, A.N. Netravali, Green resin from forestry waste residue “karanja (pongamia pinnata) seed cake” for biobased composite structures, ACS Sustain. Chem. Eng. 2 (2014) 2318–2328, http://dx.doi.org/10.1021/sc500095r.

[20] M.M. Rahman, K. Ho, A.N. Netravali, Bio-based polymeric resin from agricultural waste, neem (Azadirachta indica) seed cake, for green composites, J. Appl. Polym. Sci. 132 (2015), http://dx.doi.org/10.1002/app.41291 n/a–n/a.

[21] F. Song, D.-L. Tang, X.-L. Wang, Y.-Z. Wang, Biodegradable soy protein isolate-based materials: a review, Biomacromolecules 12 (2011) 3369–3380, http://dx.doi.org/10.1021/bm200904x.

[22] M.M. Rahman, A.N. Netravali, B.J. Tiimob, V. Apalangya, V.K. Rangari, Bio-inspired “green” nanocomposite using hydroxyapatite synthesized from eggshell waste and soy protein, J. Appl. Polym. Sci. 133 (2016), http://dx.doi.org/10.1002/app.43477 n/a–n/a.

[23] X. Huang, A. Netravali, Characterization of flax fiber reinforced soy protein resin based green composites modified with nano-clay particles, Compos. Sci. Technol. 67 (2007) 2005–2014, http://dx.doi.org/10.1016/j.compscitech.2007.01.007.

[24] P. Lodha, A.N. Netravali, Characterization of interfacial and mechanical properties of “green” composites with soy protein isolate and ramie fiber, J. Mater. Sci. 37 (2002) 3657–3665, http://dx.doi.org/10.1023/A:1016557124372.

[25] S. Nam, A.N. Netravali, Characterization of ramie fiber/soy protein concentrate (SPC) resin interface, J. Adhes. Sci. Technol. 18 (2004) 1063–1076, http://dx.doi.org/10.1163/1568561041257504.

[26] J.T. Kim, A.N. Netravali, Effect of protein content in soy protein resins on their interfacial shear strength with ramie fibers, J. Adhes. Sci. Technol. 24 (2010) 203–215, http://dx.doi.org/10.1163/016942409X12538812532159.

[27] K. Qiu, A.N. Netravali, Bacterial cellulose-based membrane-like biodegradable composites using cross-linked and noncross-linked polyvinyl alcohol, J. Mater. Sci. 47 (2012) 6066–6075, http://dx.doi.org/10.1007/s10853-012-6517-9.

[28] A. Nakayama, A. Kakugo, J.P. Gong, Y. Osada, M. Takai, T. Erata, S. Kawano, High mechanical strength double-network hydrogel with bacterial cellulose, Adv. Funct. Mater. 14 (2004) 1124–1128, http://dx.doi.org/10.1002/adfm.200305197.

[29] S. Iwamoto, A. Isogai, T. Iwata, Structure and mechanical properties of wet-spun fibers made from natural cellulose nanofibers, Biomacromolecules 12 (2011) 831–836, http://dx.doi.org/10.1021/bm101510r.

[30] A. Retegi, N. Gabilondo, C. Peña, R. Zuluaga, C. Castro, P. Gañan, K. de la Caba, I. Mondragon, Bacterial cellulose films with controlled microstructure–mechanical property relationships, Cellulose 17 (2009) 661–669, http://dx.doi.org/10.1007/s10570-009-9389-7.

[31] J. Kováčik, Correlation between Young's modulus and porosity in porous materials, J. Mater. Sci. Lett. 18 (n.d.) 1007–1010. doi:10.1023/A:1006669914946.

[32] M.M. Rahman, S. Zainuddin, M.V. Hosur, J.E. Malone, M.B.A. Salam, A. Kumar, S. Jeelani, Improvements in mechanical and thermo-mechanical properties of e-glass/epoxy composites using amino functionalized MWCNTs, Compos. Struct. 94 (2012) 2397–2406, http://dx.doi.org/10.1016/j.compstruct.2012.03.014.

[33] H. Sai, L. Xing, J. Xiang, L. Cui, J. Jiao, C. Zhao, Z. Li, F. Li, T. Zhang, Flexible aerogels with interpenetrating network structure of bacterial cellulose–silica composite from sodium silicate precursor via freeze drying process, RSC Adv. 4 (2014) 30453–30461, http://dx.doi.org/10.1039/C4RA02752C.

[34] A.N. Nakagaito, H. Yano, The effect of fiber content on the mechanical and thermal expansion properties of biocomposites based on microfibrillated cellulose, Cellulose 15 (2008) 555–559, http://dx.doi.org/10.1007/s10570-008-9212-x.

[35] A. Retegi, I. Algar, L. Martin, F. Altuna, P. Stefani, R. Zuluaga, P. Gañán, I. Mondragon, Sustainable optically transparent composites based on epoxidized soy-bean oil (ESO) matrix and high contents of bacterial cellulose (BC), Cellulose 19 (2011) 103–109, http://dx.doi.org/10.1007/s10570-011-9598-8.

[36] H.L. Cox, The elasticity and strength of paper and other fibrous materials, Br. J. Appl. Phys. 3 (1952) 72, http://dx.doi.org/10.1088/0508-3443/3/3/302.

[37] M.M. Rahman, M. Hosur, S. Zainuddin, N. Jahan, E.B. Miller-Smith, S. Jeelani, Enhanced tensile performance of epoxy and E-glass/epoxy composites by randomly-oriented amino-functionalized MWCNTs at low contents, J. Compos. Mater. 49 (2015) 759–770, http://dx.doi.org/10.1177/0021998314525977.

[38] D.G. Harlow, S.L. Phoenix, The chain-of-bundles probability model for the strength of fibrous materials I: analysis and conjectures, J. Compos. Mater. 12 (1978) 195–214, http://dx.doi.org/10.1177/002199837801200207.